On improving process efficiency and weld quality in ultrasonic welding of misaligned thermoplastic composite adherends

B. G. Brito, C.; Teuwen, J.; Dransfeld, C. A.; F. Villegas, I.

DOI
10.1016/j.compstruct.2022.116342

Publication date
2023

Document Version
Final published version

Published in
Composite Structures

Composite Structures 304 (2023) 116342

Contents lists available at ScienceDirect

Composite Structures

journal homepage: www.elsevier.com/locate/compstruct

On improving process efficiency and weld quality in ultrasonic welding of misaligned thermoplastic composite adherends

C. B. G. Brito *, J. Teuwen, C.A. Dransfeld, I. F. Villegas

Aerospace Structures and Materials Department, Faculty of Aerospace Engineering, Delft University of Technology, Kluyverweg 1, 2629 HS Delft, the Netherlands

ARTICLE INFO

Keywords:
Fusion bonding
Welding force
Energy director
Carbon fibre
Porosity
Joints/joining

ABSTRACT

This paper evaluates the potential of changing the welding force and the compliance of the energy director (ED) to reduce the effects caused by misaligned adherends, which were: increased through-thickness heating, reduced size of welded area and increased heating time. In the methodology that was followed, we welded adherends misaligned by approximately 4.5° in different scenarios: with higher welding force; with increased ED compliance by the use of a thicker ED and; with increased ED compliance by the use of a discontinuous ED. The most significant reduction of the effects caused by misaligned adherends was obtained when combining the use of both increased welding force and discontinuous ED. Such improvement derives from the imposed parallelism caused by the use of a higher welding force and from a more efficient concentration of heat generation at the weld line that occurs when a discontinuous ED is used.

1. Introduction

Thermoplastic composites provide some advantages over thermoset composites, such as higher resistance to impact [1,2,3], ease of manufacturing (such as hot press forming), weldability and recyclability. Due to these advantages, thermoplastic composites have been increasingly used in aerospace industry, as demonstrated by Airbus with its thermoplastic composites leading edge of the A340-600 [4] in early 2000 and by Gulfstream that used thermoplastic composites in critical control surfaces of the G650 [5] in 2012. To assemble these thermoplastic parts together, different welding techniques were employed, such as resistance welding by Airbus and induction welding by Gulfstream.

In addition to resistance and induction welding, ultrasonic welding is a welding technique with great potential to be used in aerospace applications. In ultrasonic welding, a sonotrode is used to apply a static force on the parts to be welded together while simultaneously exerting high frequency, low amplitude vibrations on them [6,7,8]. During the vibration phase, the ultrasonic vibrations are responsible for the interfacial friction and viscoelastic heating mechanisms [9,10] that result in very fast processing times. Besides that, no foreign material is needed at the welding interface. Instead, a resin-rich element called *energy director* (ED) is placed between the joining parts in order to focus the heat generation at the welding interface [6,7,11,12,13]. Once the energy director is molten, the sonotrode squeezes it out and molecular interdiffusion of the polymer chains of the locally molten adherends establishes the bond. A consolidation phase takes place after that, where a static force is applied on the welded parts for a certain period of time to prevent deconsolidation. The high energy-efficiency and the possibility of in-situ monitoring [6,14,15,16] also make ultrasonic welding a promising technique for the next generation of aircrafts, which aims to increase production rate and to reduce fuel emissions and costs [17].

The ultrasonic welding process can be either static or continuous. The static process differs from the continuous one because the size of the area that can be welded at once is limited to the size of the sonotrode in the former. Meanwhile, longer seams can be obtained in continuous ultrasonic welding because the sonotrode moves along the parts to be welded [18]. To upscale the ultrasonic welding process, understanding how the static process is affected when subjected to real-life conditions is essential before moving on to the continuous process. In our previous work [19], we used C/PEEK adherends to show the effects that a misalignment between them has on the heat generation of the static process and on the quality of the final welds. Through-thickness heating on the adherends was observed and related to the lack of contact between the energy director and the adherends, which results in the amplitude of vibration being transmitted exclusively to the top adherend. Also, a decrease in the size of the welded area and in the uniformity of the quality of the weld occurred, which was related to the hindered frictional heating at the over-compressed edge of the overlap. Finally,

* Corresponding author.
E-mail address: c.brito@tudelft.nl (C. B. G. Brito).

https://doi.org/10.1016/j.compstruct.2022.116342
Received 13 June 2022; Received in revised form 13 September 2022; Accepted 7 October 2022
Available online 15 October 2022

the reduced amplitude of vibration reaching the energy director increased the heating time of the static ultrasonic welding process.

In order to ensure that ultrasonic welding of thermoplastic composite parts can be industrialized and upscaled, its performance, adaptability and resilience to unideal industrial scenarios has to be investigated. Therefore, a few approaches to reduce the abovementioned effects that arise from the presence of an angle between the adherends are considered. For instance, Jongbloed et al. [13] showed that using a more compliant energy director (a woven polymer mesh instead of a film) in continuous ultrasonic welding improved the uniformity of the welded area due to its better contact with the C/PPS adherends as a result of the energy director larger deformation. Although the adherends used by the authors were parallel to each other, we believe that the increased deformation has the potential to improve the transmission of the amplitude of vibration to the energy director when a misalignment is present. Another way to increase the compliance of the energy director is by increasing its thickness. Palardy and Villegas [12] studied three energy director thicknesses for static ultrasonic welding of C/PEI adherends. The authors concluded that heating and melting of the adherends and the energy director occur simultaneously for a 0.06 mm-thick energy director, which is a premature heating of the adherends when compared to the cases where thicker energy directors (0.25 mm and 0.50 mm) are used. Besides that, signs of overheating and degradation were found on the fracture surface of the thinner energy director even for optimum conditions, which did not occur for the larger thicknesses, showing the potential that increasing the energy director thickness has on preventing early heating of the adherends.

To improve the contact between the energy director and the adherends and to potentially reduce the through-thickness heating on the adherends, another alternative is to increase the welding force applied during the process, as demonstrated by the work of Villegas [14]. The increased force and consequent increased intimate contact between ED and adherends also made the process faster, resulting in a shorter heating time than when a lower welding force was used. According to Villegas, the improvement of intimate contact occurred at a microscopic level, as the C/PEI adherends used by the author were parallel to each other. In our case, we believe that if a high enough force is employed, it will compel the top adherend towards the energy director and impose parallelism between the adherends along the overlap, improving contact with the energy director and reducing the heating time.

Therefore, our objective is to investigate how increasing the welding force and increasing the energy director compliance in misaligned adherends affect through-thickness heating in the adherends, the size of the welded area and the heating time of the process, since all the above mentioned studies focus only on a parallel configuration. It is expected that increasing the welding force improves the transmission of the vibration amplitude to the ED, reducing through-thickness heating in the adherends, unwelded area and heating time. A similar result regarding the through-thickness heating is expected when increasing the ED compliance due to the increased contact between ED and adherend. Cross-sectional microscopy and C-scan inspection were used to qualitatively evaluate the extent of through-thickness heating in the adherends and fracture surface analysis was used to assess the amount of welded area and the general state of the material in the weld line. Single-lap shear strength tests and scanning electron microscopy were performed to further assess the quality of the welds. This investigation contributes to the maturation of ultrasonic welding as a robust and reliable joining method in the composite field.

2. Methodology

2.1. Materials and manufacturing

The specimens used in this paper were made of polyetheretherketone (C/PEEK) reinforced with carbon 5-harness satin fabric from Toray Advanced Composites (the Netherlands). The prepreg had 50% nominal fibre volume content and the type of the carbon fibre was T300JB. The laminates were stacked in a $[(0/90)_3]_s$ sequence and consolidated in a hot platen press at 385 °C and 10 bar for 30 min. The nominal thickness of the consolidated laminate was 1.90 mm. From the laminate, adherends measuring 25.4 mm by 101.6 mm were cut with a water-cooled diamond blade. They were cut with their longitudinal edge parallel to the main apparent orientation of the fibres.

Three different types of ED were used: 0.25 mm-thick continuous film, 0.50 mm-thick continuous film and 0.40 mm-thick discontinuous film. The difference between the continuous and the discontinuous films is that the former is a continuous piece of material while the latter presents open areas, as schematically represented in Fig. 1. The three types of ED were made out of neat PEEK. For the 0.25 mm-thick and 0.50 mm-thick continuous films, one or two layers of a 0.25 mm-thick film supplied by Goodfellow Cambridge Ltd (England) were used, respectively. In the case of the 0.50 mm-thick, the two 0.25 mm-thick films were stacked on top of each other, placed on the overlap and held in place by an adhesive tape. For the discontinuous energy director, one layer of 0.40 mm-thick discontinuous film with an areal weight of 149 g/m^2 supplied by Dexmet Corporation (USA) was used. The compliance of each ED type (see Table 1), C, was calculated through the following equation:

$$C = \frac{L_{ED}}{A_{ED}E_{ED}} \tag{1}$$

where L_{ED} is the ED thickness, A_{ED} is the amount of area covered by the ED within the overlap based on full contact and E_{ED} is the elastic modulus of the ED, which is 3.7GPa based on the material's datasheet [20].

2.2. Ultrasonic welding process

A 20 kHz ultrasonic welding machine (HiQ DIALOG SpeedControl) from Herrmann Ultraschall, Germany, was used to weld the adherends in a single-lap configuration (overlap of 12.7 mm length and 25.4 mm width). The sonotrode had a rectangular contact area of 15 mm by 30 mm. A peak-to-peak amplitude of vibration of 86.2 μm was used in all cases. The welding force varied depending on the case, being either 500 N or 1500 N. Fig. 2 shows the jig used to prevent the movement of the adherends during the static ultrasonic welding process. The jig consists of two metal bars used to clamp each adherend to the base of the anvil. The distance between the sonotrode and the clamp holding the bottom adherend was kept at 25 mm for all cases. The distance between the sonotrode and the clamp holding the top adherend, the *clamping distance* in Fig. 2, affects the misalignment between the adherends and the compliance of the top adherend [19]. This distance was kept at 5 mm for all cases, except for the parallel reference for which 50 mm was used to ensure parallelism. A supporting base is usually used under the top adherend to ensure parallelism between the adherends (see Fig. 2). For the parallel reference, a supporting base thickness of 1.90 mm was used, while the thickness of the supporting base was either 1.50 mm or 1.25 mm to achieve a misalignment angle of approximately 4.50° for all the other cases. Such angle and clamping distance were chosen because they resulted in the most severe angle effects (smallest welded area, largest through-thickness heating and longest heating time) according to our previous work [19].

The vertical displacement of the sonotrode was used to indirectly control the duration of the vibration phase. The ultrasonic welding process was stopped at two distinct moments, depending on the analyses to be conducted. These moments were the *onset of the flow* and the *optimum displacement*. The onset of the flow is defined by the start of the downward movement of the sonotrode and it is related to the beginning of the squeeze flow of the molten material out of the welding overlap [14]. The onset of the flow provides important insight regarding heat generation and it allows a more consistent comparison between different

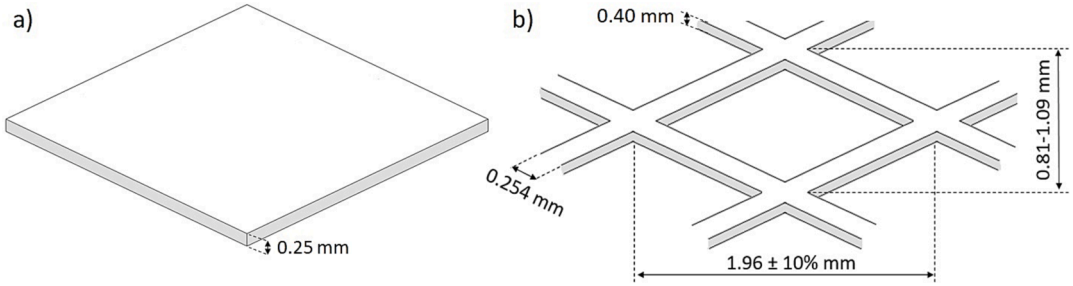

Fig. 1. Schematic of the a) continuous and b) discontinuous films.

Table 1
Summary of the different ED types with respective thickness (L_{ED}), area covered by the ED within the overlap (A_{ED}) and compliance (C).

ED type	L_{ED} [mm]	A_{ED} [mm^2]	C [mm/N]0.10^{-7}
Continuous	0.25	322.58	2.09
	0.50	322.58	4.19
Discontinuous	0.40	224.13	4.90

cases. The displacement at the onset of the flow was defined as 0.03 mm for all cases due to practical reasons. No consolidation pressure was applied after the vibration phase to prevent further squeeze flow due to the application of the consolidation pressure.

Optimum displacement is defined as that which results in welds with the highest strength. The optimum displacement varies depending on the material, on the ED type and on the welding parameters. The work of Villegas [14] describes five stages during the ultrasonic welding process, which are determined by using the power and displacement outputs from the welder machine. The optimum displacement is found within the fourth stage, where melting of the first layer of the adherends starts to occur. The procedure described by Villegas [14] was used to determine the optimum displacement for the cases that presented a similar power curve as the one described by the author. When the power curves presented a different profile, a range of displacements was tested to defined the optimum displacement. Because welds made with misaligned adherends show a non-uniform fracture surface [19], we also considered the absence of signs of overheating on the fracture surface (such as discoloration of the resin and misalignment of the fibre bundles) as a required criteria to determine the optimum displacement of each case. The duration of the vibration phase and the corresponding consumed energy for each optimum displacement are called *optimum time* and *optimum energy*, respectively. For the welds obtained at optimum displacement, a consolidation pressure of 500 N was applied for 4 s to avoid deconsolidation in the weld line and in the adherends.

2.3. Angle and contact area measurement

The angle between adherends was measured using high-resolution pictures of the overlap (Optomotive high-resolution digital camera, Mechatronics Ltd) post-processed with ImageJ software (version 1.52a). In some cases, due to the larger size of the ED in comparison to the overlap, the ED could partially block the view of the longitudinal edges of the adherends that are adjacent to the overlap. Due to this issue, the outer longitudinal edges of the adherends were used to measure the angle, as indicated in Fig. 3. For each case, three different sets of bottom adherend, ED and top adherend were used. The transverse edges of the overlap are referred to as E1 (Edge 1) and E2 (Edge 2) hereafter, where E1 and E2 correspond to the free edge of the top and of the bottom adherend, respectively (Fig. 3).

Our previous work [19] showed that the contact area between the sonotrode and the top adherend is a way to quantify the degree of misalignment between the adherends under the welding force. This quantification provides information about the amplitude of vibration that is transmitted to the *welding stack* (top adherend-ED-bottom adherend). Therefore, we measured the contact area for the different cases studied in this paper. For that, a double-sided adhesive tape with a thickness of 0.15 mm was placed on the top surface of the top adherend

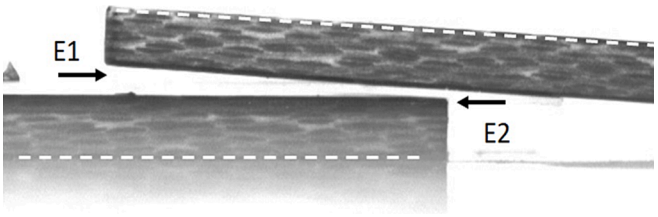

Fig. 3. Side view of the overlap where the dashed lines correspond to the adherends' outer surfaces used to measure the angle between them. The transverse edges of the overlap, E1 and E2, are also indicated.

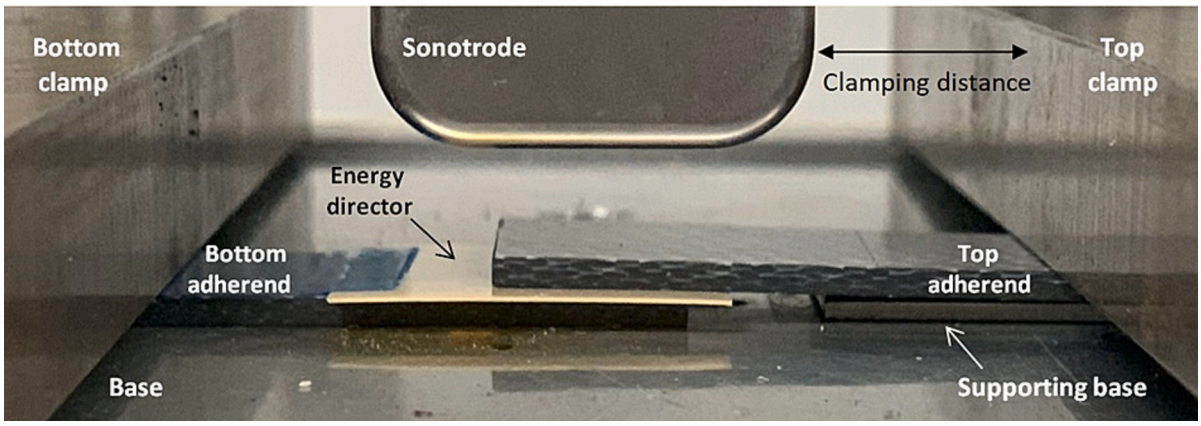

Fig. 2. Static ultrasonic welding process set-up.

while the bottom surface of the sonotrode was painted with a marker pen. The sonotrode was moved down until the prescribed welding force was applied to the welding stack and then moved back to its retracted position. When the sonotrode applied the welding force on the welding stack, the paint on the bottom surface of the sonotrode was transferred to the adhesive tape where contact occurred, allowing the observation of the imprint of the contact area once the sonotrode returned to its retracted position. Three sets of bottom adherend, ED and top adherend were used to obtain the imprint of the contact area for each case and a calliper was used to measure its dimensions in three different positions along the width of the imprint.

2.4. Testing and analysis

To analyse the through-thickness heating on the adherends, ultrasonic through-transmission C-scan inspection and cross-section microscopy were performed. For the C-scan, an Olympus OmniScan SX was used to scan the samples, which were immersed in a water tank, between the emitter and the receiver transducers of the equipment. To prevent water from entering the voids and potentially interfering with the results of the inspection, the edges around the overlap of all samples were sealed with Vaseline®. For the cross-sections, the overlap was cut along the longitudinal direction of the adherends, at the centre of the adherends width. The samples were then embedded in epoxy resin and a Struers Tegramin-20 polisher was used. A Keyence VH-Z100UR digital microscope was used to observe and analyse the cross-sections. Since the C-scan shows where porosity is located over the overlap area and the cross-section micrograph shows how deep that porosity has spread from the welding interface into the adherends, the techniques were used together to provide a more complete overview of the distribution of porosity on the welded joint.

The strength of the welds was measured via single-lap shear tests and the fracture surfaces were analysed after the mechanical tests. A Zwick/Roell 250kN universal testing machine with a crosshead speed of 1.3 mm/min was used for the mechanical tests. The lap shear strength (LSS) was calculated by dividing the maximum load registered in the test by the total overlap area (12.7 mm × 25.4 mm). This LSS is referred to as *apparent LSS* from now on. The welded area was measured using a Keyence One-shot 3D Measuring Macroscope VR-3000 Series. Hence a second LSS, referred to as *effective LSS* from now on, was then calculated by dividing the maximum load registered in the test by the measured welded areas instead of the overlap area. To evaluate the fracture surfaces, naked-eye inspection and scanning electron microscopy (JEOL JSM-7500F Field Emission Scanning Electron Microscope, SEM) were performed after the mechanical tests.

Table 2 shows the nomenclature used throughout this work for each case and Table 3 shows a summary of the parameters used for the cases.

To verify the statistical relevance that the different approaches had on the LSS with respect to the REF(A), which is the case that we want to improve, we carried out an one-way analysis of variance (ANOVA). Two parameters were of main interest when performing ANOVA: the *F value*, which determines if the variance between the means of two populations is significantly different, and the *p value* (significance level), which indicates the probability of the results to have occurred by chance. The null hypothesis, i.e. if the results were statistically equal, was rejected for $p < 0.05$.

Table 2
Summary of the nomenclature used for the different cases.

Nomenclature	Definition
REF(P)	Reference (REF) for parallel adherends (P)
REF(A)	Reference (REF) for welds with misaligned adherends (A)
HF(A)	Higher welding force (HF) for welds with misaligned adherends (A)
TED(A)	Thicker ED (TED) for welds with misaligned adherends (A)
DED(A)	Discontinuous ED (DED) for waelds with misaligned adherends (A)
DED-HF(A)	Discontinuous ED (DED) and higher welding force (HF) for welds with misaligned adherends (A)

3. Results

3.1. Analytical calculation of cyclic strain and through-thickness deformation

For the different cases obtained with each type of ED, we calculated the *ideal* through-thickness strain and through-thickness deformation on the ED and on the adherends and the strain ratio between them. For that, we used an analytical model where an ideal configuration, i.e. parallel adherends, was assumed and in which only the portion of the elements within the overlap area is considered and modelled as an association of springs in series [21]. For the cases with a continuous ED, the strain of the ED, ε_{ED}, and on the adherends, ε_{Ad}, is expressed by:

$$\varepsilon_{ED} = \frac{\Delta L}{\left[2\frac{E_{ED}}{E_{Ad}}L_{Ad} + L_{ED}\right]} \tag{2}$$

and

$$\varepsilon_{Ad} = \frac{\Delta L}{\left[\frac{E_{Ad}}{E_{ED}}L_{ED} + 2L_{Ad}\right]} \tag{3}$$

where L is the element thickness (either the ED (subscript ED) or the adherends (subscript Ad)) and ΔL is the total deformation on the welding stack (hence half-peak of the amplitude of vibration, 43.1 μm).

In the case of the discontinuous ED, the area covered by the ED (A_{ED}) is smaller than the overlap area (A_{Ad}), hence ε_{ED} and ε_{Ad} are expressed by:

$$\boldsymbol{\varepsilon_{ED}} = \frac{\Delta \boldsymbol{L}}{\left[2\frac{\boldsymbol{E_{ED}A_{ED}}}{\boldsymbol{E_{Ad}A_{Ad}}}\boldsymbol{L_{Ad}} + \boldsymbol{L_{ED}}\right]} \tag{4}$$

and

$$\varepsilon_{Ad} = \frac{\Delta L}{\left[\frac{E_{Ad}A_{Ad}}{E_{ED}A_{ED}}L_{ED} + 2L_{Ad}\right]} \tag{5}$$

The amount of area covered by the ED within the overlap, A_{ED}, was shown in Table 1. As already mentioned, the value of 3.7GPa was used for the elastic modulus of a PEEK ED, according to the material's datasheet [20]. To simplify the analytical model, the composite adherend is assumed isotropic [10]. Therefore, the value of 11GPa was used as the transverse elastic modulus of the adherends based on the rule of mixtures that assumes 180GPa as the elastic modulus of the carbon fibres [10]. Once the strain in each element is known, the analytical deformation on them can be calculated by:

$$\Delta L_{ED} = \varepsilon_{ED} L_{ED} \tag{6}$$

and

$$\Delta L_{Ad} = \varepsilon_{Ad} L_{Ad} \tag{7}$$

Table 4 shows the thickness (L), the overlap area (A_{Ad}), the analytical values of deformation (ΔL) and through-thickness strain (ε) on each element and the strain ratio ($\boldsymbol{\varepsilon_{ED}}/\boldsymbol{\varepsilon_{Ad}}$) between ED and adherends for the different ED types tested in this paper when the vibration is applied. These calculations could have been performed with a numerical simulation, which would also allow the estimation of the deformation and strain for misaligned cases. However, because we believe that the results from the analytical calculations for the parallel cases can be extrapolated to the misaligned cases as a first approximation, with the advantage of sparing the time that would be needed to create and validate the model, we decided to not use the numerical approach in this study.

Table 3
Summary of tests.

Case	ED type	ED thickness [mm]	Welding Force [N]	Angle [°]	Study	Number of samples	Clamping distance [mm]	Base thickness [mm]
REF(P)	Continuous	0.25	500	0.45 ± 0.18	LSS	4	50	1.90
REF(A)	Continuous	0.25	500	4.45 ± 0.27	Oof[1]	2	5	1.25
					LSS	4		
HF(A)	Continuous	0.25	1500	4.45 ± 0.27	LSS	4	5	1.25
TED(A)	Continuous	0.50	500	4.52 ± 0.08	Oof[1]	2	5	1.50
					LSS	5		
DED(A)	Discontinuous	0.40	500	4.80 ± 0.20	LSS	5	5	1.25
DED-HF(A)	Discontinuous	0.40	1500	4.80 ± 0.20	LSS	4	5	1.25

[1] refers to Onset of the flow, defined in this work as a downward displacement of the sonotrode = 0.03 mm.

Table 4
Thickness (L), overlap area (A_{Ad}), analytical deformation (ΔL), and through-thickness strain (ε) on each element and the strain ratio between both ($\boldsymbol{\varepsilon_{ED}/\varepsilon_{Ad}}$) for different types of energy director assuming a parallel configuration.

ED type	Continuous		Discontinuous
L_{ED} [mm]	0.25	0.50	0.40
ΔL_{ED} [mm]0.10^{-5}	0.7	1.2	1.3
ε_{ED} [-]	0.0282	0.0242	0.0335
A_{Ad} [mm^2]	322.58	322.58	322.58
L_{Ad} [mm]	1.90	1.90	1.90
ΔL_{Ad} [mm]0.10^{-5}	1.8	1.6	1.5
ε_{Ad} [-]	0.0095	0.0082	0.0078
$\varepsilon_{ED}/\varepsilon_{Ad}$[-]	2.97	2.95	4.29

3.2. Assessment of the porosity in the welds

Fig. 4 shows the C-scan results of welds obtained with the parameters that yielded the highest strength for REF(P), REF(A), HF(A), TED(A), DED(A) and DED-HF(A). The areas with the highest attenuation in the wave signal can be seen at Edge 1 in the overlap of REF(A) and TED(A), followed by DED(A).

Fig. 5 shows the cross-sectional micrograph of welds obtained with the parameters that yielded the highest strength for all the cases in this study. Intact ED and adherends are seen at E2 of the overlap in all cases. Among the different approaches to mitigate the through-thickness heating in the adherends, TED(A) is the only one that presents more porosity than REF(A).

3.3. Welded area

Fig. 6 shows the corresponding fracture surfaces of the welds obtained with the parameters that yielded the highest strength for all the cases in this study. One can see that only REF(P) has the whole overlap area welded while all other cases present some reduction in the welded area, being HF(A) and DED-HF(A) with 82% of the overlap area welded, followed by DED(A) (77%), TED(A) (71%) and REF(A) (44%). Despite the size of the welded area, all cases present first-ply failure in the C/PEEK adherend, with exception of cases HF(A) and DED-HF(A) that also present second-ply failure in the C/PEEK adherend.

3.4. Lap-shear strength and processing parameters

Table 5 shows the contact area and summarizes the processing parameters that yielded the highest strength welds for each case studied in this paper.

Fig. 7 plots the contact area, the welded area, the apparent and the effective LSS of the highest strength welds of each case, while Table 6 shows the ANOVA results for the effective LSS of cases HF(A), TED(A), DED(A) and DED-HF(A) with respect to case REF(A). One can see that the size of the welded area increased for all cases in comparison to REF (A), but remained below the values of REF(P). The apparent LSS also increased for all cases in comparison to REF(A), with the exception of TED(A), but remained below REF(P).

Fig. 8 plots the optimum time and optimum energy for all the cases in this study. One can see that both the optimum time and energy of cases HF(A) and DED-HF(A) considerably decreased in comparison to REF(A) or to the other two approaches, almost reaching values similar to REF (P).

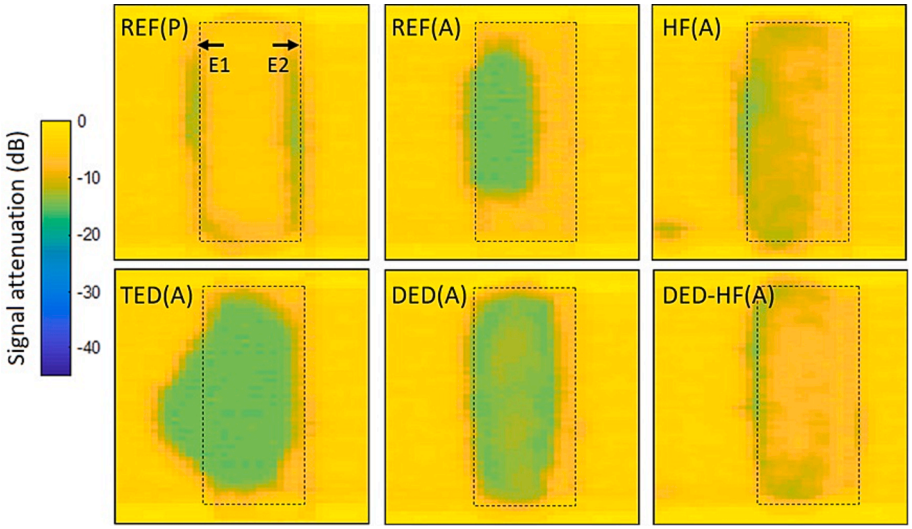

Fig. 4. C-scan of the overlap area of welded samples for each case.

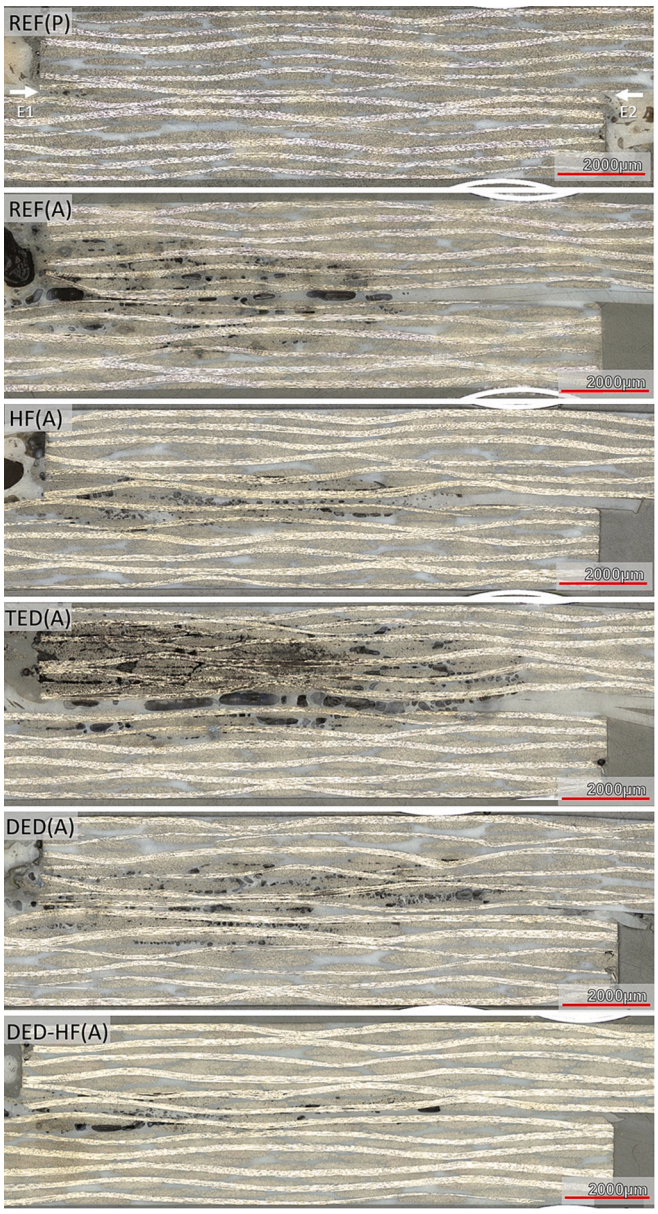

Fig. 5. Longitudinal cross-section micrographs of each case.

4. Discussion

To understand the effect of the different approaches on the through-thickness heating in misaligned adherends, we used C-scan inspection and looked at cross-section micrographs of the different cases at the displacement that yielded the highest strength welds. For HF(A), the increased welding force reduced the through-thickness heating in the adherends, as it can be seen by the relatively low attenuation observed in the C-scan and by the limited porosity in the cross-section micrograph (Fig. 4.c and Fig. 5.c, respectively) as compared to REF(A) (Fig. 4.b and Fig. 5.b). The reduced through-thickness heating in the adherends is a result of the higher degree of parallelism between the adherends imposed by the higher force, as evidenced by the significant increase in contact area (i.e., contact between sonotrode and top adherend) for HF (A) as compared to REF(A) (Fig. 7). The increased parallelism increases the contact between the top adherend and the ED and hence improves the transmission of the vibration amplitude to the ED.

Increasing the compliance of the ED (TED(A) and DED(A) cases) improves the contact between the ED and the adherends towards Edge 1 due to the larger deformation of the ED (Table 4), as schematically shown in Fig. 9. As mentioned earlier, improved contact between top adherend and ED improves the transmission of the vibration to the ED. However, despite the increased deformation of the ED, the C-scan results and the cross-section micrographs of the highest strength welds presented in Fig. 4 and Fig. 5 show increased porosity for TED(A) when compared to REF(A). We believe that this relates to the fact that the highest weld strength for REF(A) is obtained *before* the onset of the flow, while the highest weld strength for TED(A) is obtained well *beyond* the onset of the flow (Table 4). Having obtained these two types of welds in different stages during the welding process hinders the comparison. Indeed, when comparing both cases at the same stage during the ultrasonic welding process, e.g., the onset of the flow, TED(A) shows less severe through-thickness heating than REF(A) (see Fig. 10). The reader should note that contrarily to Fig. 5, the cross-section micrographs shown in Fig. 10 correspond to samples that did not undergo consolidation after heating in order to prevent that further squeeze flow affected the comparison. Finally, when decreasing the overlap area covered by the ED by using a discontinuous ED (DED(A)), there is a significant increase in the strain ratio between ED and adherends compared to both the reference 0.25 mm-thick continuous ED and the 0.50 mm-thick continuous ED (see Table 4). This means that using a discontinuous ED is a more efficient way of focusing heat generation at the welding interface than using a continuous ED and results in lower through-thickness heating in the adherends for DED(A) as compared to TED(A) and REF(A), as seen in Fig. 5. Combining the use of a discontinuous ED with an increased welding force (DED-HF(A)) shows an even greater reduction in the through-thickness heating on the adherends, as shown in Fig. 4.f, where the attenuation in the wave signal is the lowest after REF(P) and in Fig. 5.f, with the least amount of porosity among all cases besides REF(P).

Regarding the size of the welded area, increasing the force and/or increasing the compliance of the ED, increased the welded area in comparison to REF(A) (Fig. 7). The welded area was, in any case, smaller than the full overlap, i.e., the welded area in the REF(P) case (see Fig. 7). The increase in welded area with regards to REF(A) resulted from the increased contact between the top adherend and the ED, as explained before. The size of the welded area directly affects the LSS of a joint. Fig. 7 and Table 6 show that the apparent LSS of HF(A), DED(A) and DED-HF(A) significantly increased in comparison to REF(A) (by approximately 45%, 65% and 77%, respectively). Part of the apparent increase in LSS might have come from the increased welded area for these cases in comparison to REF(A). Thus, the effective LSS must be used instead of the apparent one so only the area actually resisting the stress is taken into account. When the effective LSS is used, the results from ANOVA (see Table 6) show that there is no statistically significant difference between the LSS of cases HF(A), DED(A), DED-HF(A) and REF (A). The fact that the effective LSS of TED(A) remained significantly low in comparison with the other cases (Table 6, $p < 0.05$) despite of its increased welded area is believed to be a result of the rather thick and porous weld line (Fig. 5.d). Although the effective LSS of REF(A) is comparable to the LSS of the other cases, a very large standard deviation is observed as a result of the also large standard deviation for the welded area, which indicates that the REF(A) welds are rather inconsistent compared to the other cases. The effective LSS of cases HF(A), DED(A) and DED-HF(A) is still lower in comparison to REF(P) (Fig. 7). This decreased LSS is believed to be originated from other factors, such as the presence of porosity in the weld line and in the adherends (see Fig. 5). Also, HF(A), DED(A) and DED-HF(A) samples are subjected to additional peel stresses during single-lap shear testing, which originate from placing the non-parallel welded adherends (see Fig. 11) in the grips of the testing machine.

With respect to the increased optimum time and optimum energy that accompanies welds with misaligned adherends, Table 5 and Fig. 8 show that the only approach that significantly reduces these effects is the use of an increased welding force (both HF(A) and DED-HF(A)). This

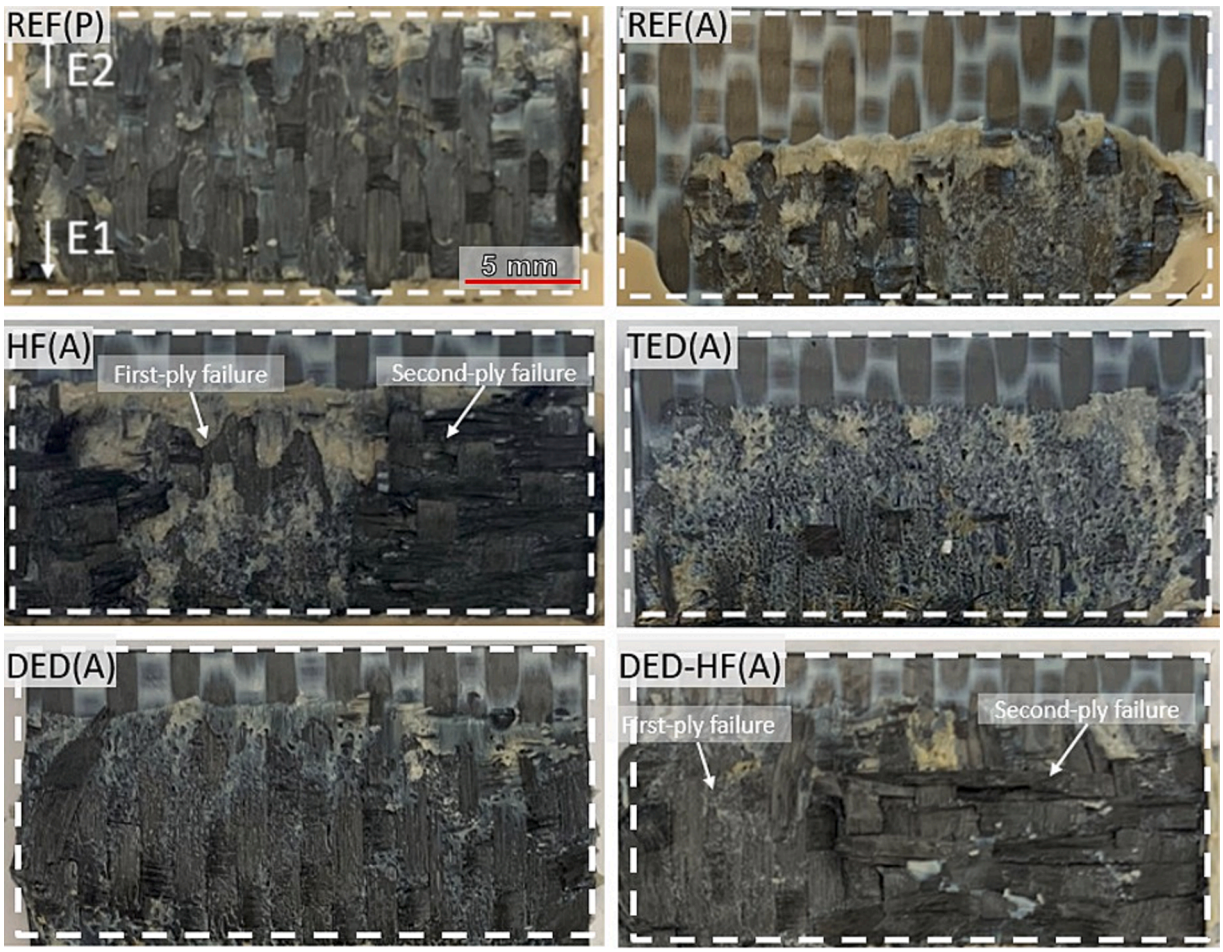

Fig. 6. Fracture surfaces of the bottom adherend of each case. Dashed rectangles indicate the overlap area.

Table 5
Different cases with their corresponding contact area and displacement (d_{LSS}), average total duration of vibration phase (t_{LSS}) and total energy (E_{LSS}) of the highest strength welds.

Case	Contact area [mm^2]	d_{LSS} [mm]	t_{LSS} [ms]	E_{LSS} [J]
REF(P)	322.58 ± 8.38	0.07	771 ± 73	1038 ± 99
REF(A)	154.94 ± 11.68	0.00*	9817 ± 2179	2200*
HF(A)	308.86 ± 9.40	0.03	1456 ± 103	1493 ± 117
TED(A)	195.07 ± 3.81	0.15	9066 ± 617	3016 ± 130
DED(A)	156.46 ± 7.87	0.20	9058 ± 1076	2687 ± 208
DED-HF (A)	276.80 ± 5.84	0.14	1278 ± 81	1419 ± 117

* The highest strength weld for REF(A) occurred before the beginning of the downward movement of the sonotrode. Thus, displacement-control could not be used and energy-control was used instead.

reduction is believed to result from the imposed parallelism caused by the increased force. The imposed parallelism not only increases the amplitude of vibration being transmitted to the ED but it also makes it more uniform along the longitudinal direction of the adherends. Therefore, an increased cyclic strain is applied to a larger portion of the ED, increasing heat generation and consequently decreasing heating time. In addition to that, the increased force increases the contact between adherends and ED, contributing to a faster melting of the material due to the nucleation of a larger number of hot spots [14]. Naturally, the more efficient transmission of the vibration amplitude reduces the energy being consumed during the process. It is important to notice that the two 0.25 mm-thick films that composed the 0.50 mm-thick ED used for TED(A) were not consolidated together, which resulted in an extra interface on the weld line for this case. Since frictional heating is one of the main heating mechanisms involved in the ultrasonic welding process, the extra interface would be expected to improve heat generation for TED(A). This potential advantage did however not result in any significant reduction of the heating time with regards to REF(A) (see Table 5 and Fig. 8).

A final aspect still has to be addressed. Although the use of a higher force and of a discontinuous ED (DED-HF(A)) considerably reduced the through-thickness heating on the adherends compared to the original case (REF(A)), porosity is still observed in the adherends (see Fig. 5). Possible hypotheses for what causes the porosity are: 1) insufficient consolidation after the vibration phase; 2) decreased volume fraction of matrix due to squeeze flow of molten resin from the adherends; 3) thermal degradation of the adherends resin and; 4) release of volatiles combined with uneven application of the consolidation force. The first hypothesis is assessed by welding case DED-HF(A) at the displacement that yielded the highest strength and applying a consolidation force of 1500 N for 60 s. Jongbloed et al. [22] showed that 5 s is enough to get the welding interface of C/PPS adherends (five harness satin weave) and woven mesh PPS ED below the glass transition temperature of PPS ($T_{g\,(PPS)}$ = 97 °C). Therefore, we assume that 60 s is a sufficient consolidation time to get our PEEK ED below its T_g ($T_{g(PEEK)}$ = 143 °C). The resulting cross-section micrograph is shown in Fig. 12, from which it is possible to observe that porosity was not eliminated. Thus, insufficient consolidation does not seem to be the source of the remaining porosity in the adherends of case DED-HF(A).

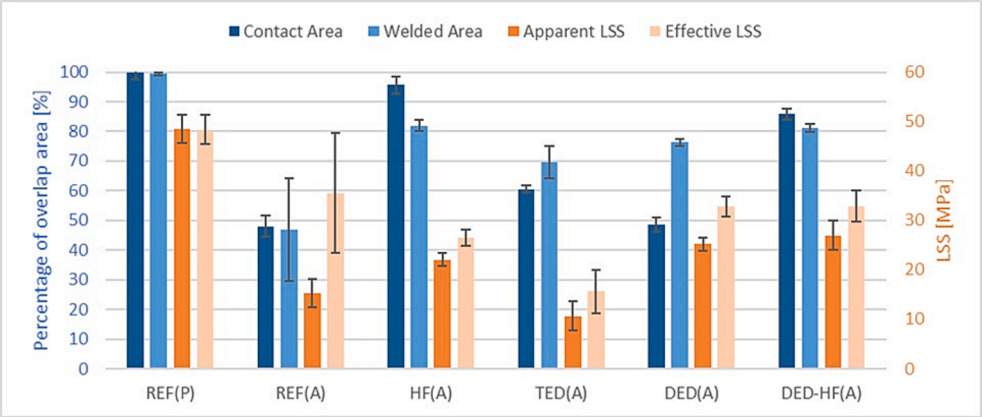

Fig. 7. Contact area, welded area, apparent and effective LSS of the different cases studied in this work.

Table 6
Effective single-lap shear strength (LSS) values for REF(A) and for the four approaches studied in this work and their ANOVA results (F-value, degrees of freedom and p-value) with respect to REF(A).

Case	Effective LSS [MPa]	ANOVA results
REF(A)	38.55 ± 12.80	–
HF(A)	26.44 ± 1.61	$F(1,7) = 2.63$, $p = 0.15$
TED(A)	15.60 ± 4.34	$F(1,7) = 12.79$, $p = 0.009$
DED(A)	32.27 ± 2.16	$F(1,6) = 0.20$, $p = 0.67$
DED-HF(A)	31.48 ± 4.37	$F(1,6) = 0.18$, $p = 0.69$

To assess the other hypotheses, SEM images of the fracture surfaces of case DED-HF(A) were evaluated. For the hypothesis regarding a decreased volume fraction of the matrix, a higher concentration of voids closer to E1, where most squeeze flow should occur, would be expected. However, the cross-section micrograph presented in Fig. 12 do not show a higher concentration of voids near E1. In the case of thermal degradation, bare fibres would be expected, being accompanied by the embrittlement of the matrix, as reported by Palardy and Villegas [12] when describing the thermal degradation of PEI. Fig. 13.a shows that fibres remain covered by resin, while Fig. 13.b shows a rather ductile aspect of a resin-rich region on the fracture surface of DED-HF(A), contrarily to a brittle behaviour. The last explanation is hypothesised based on the shape, size and distribution of the voids, suggesting that they are caused by the release of volatiles during the process, and on the

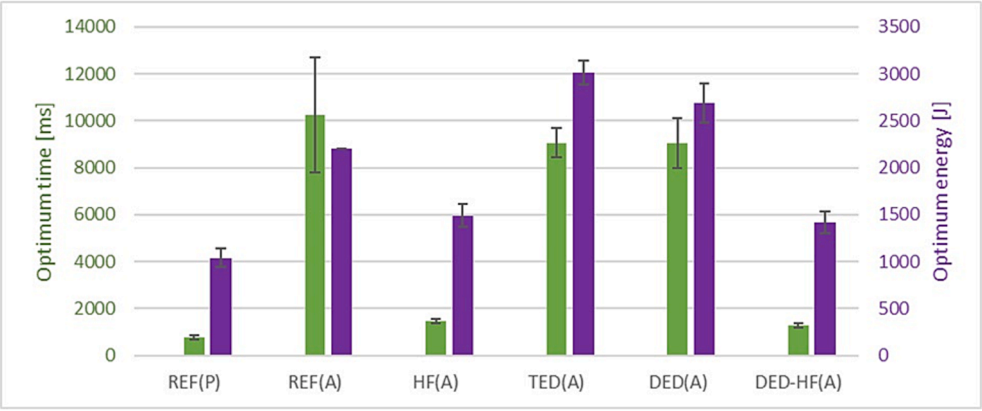

Fig. 8. Optimum time and optimum energy for all the cases in this study.

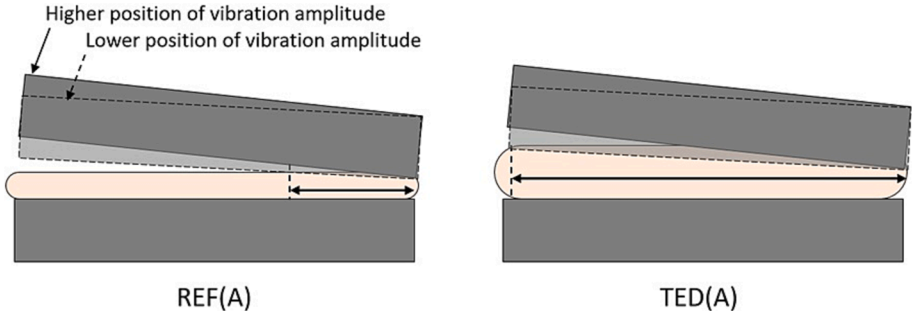

Fig. 9. Schematic of the wetting at the interface for cases REF(A) and TEF(A). The double-arrow indicates the extend of ED volume that is in contact with the top adherend at some point during the vibration.

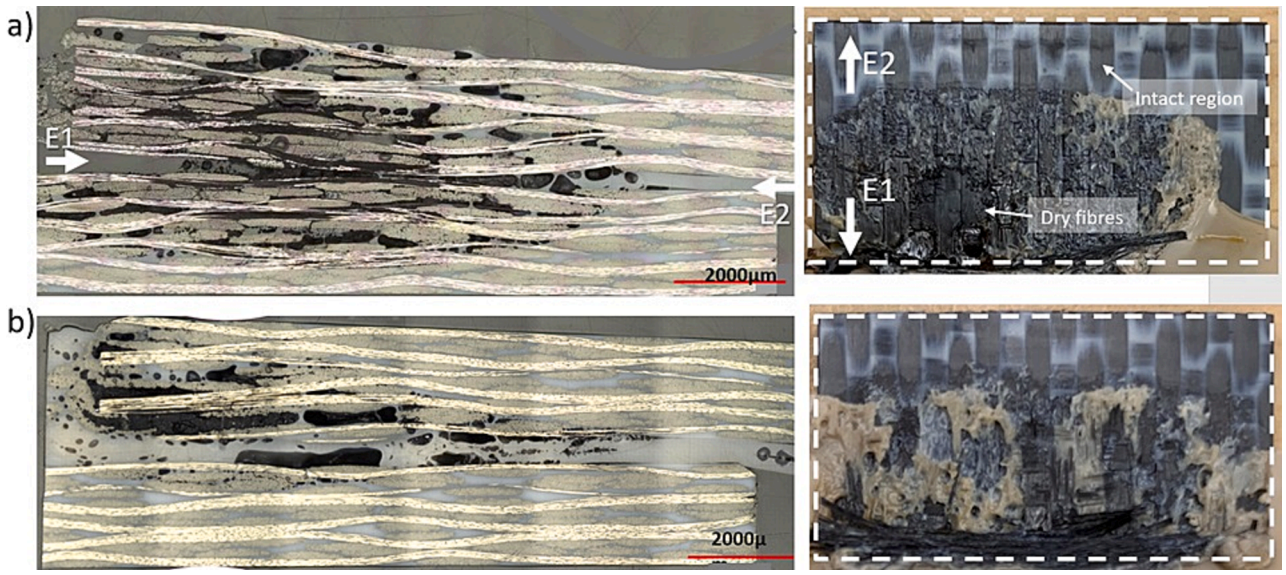

Fig. 10. Longitudinal cross-section and fracture surface of unconsolidated welds stopped at the onset of the flow of a) REF(A) and b) TED(A).

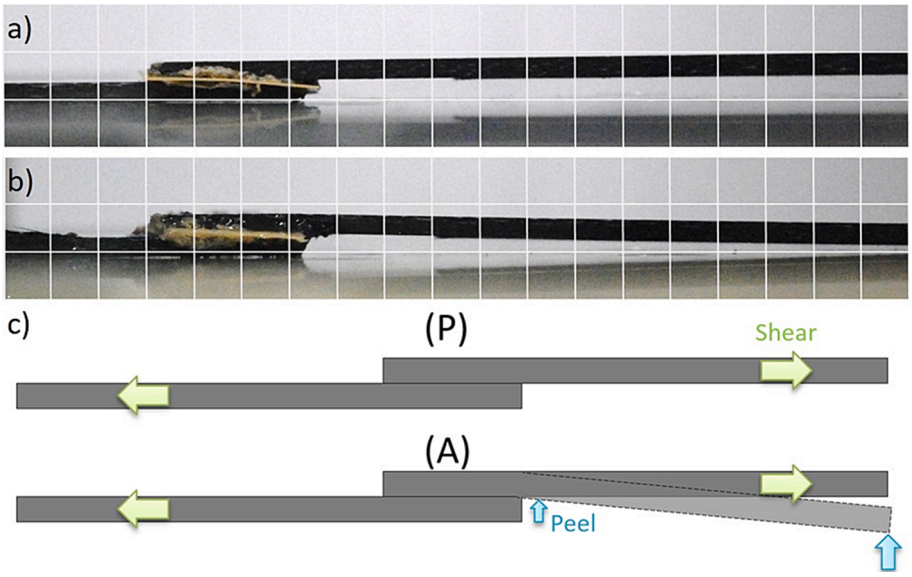

Fig. 11. Side-view of welded samples of a) REF(P) and b) HF(A) and c) schematic of LSS tests for parallel cases (P) and for cases with an angle (A) where peel stress is introduced.

Fig. 12. Longitudinal cross-section micrographs of the highest strength weld for case DED-HF(A) with consolidation force of 1500 N applied for 60 s.

constraint imposed on the downward movement of the sonotrode by the intact energy director at E2. Since the sonotrode is not infinitely rigid, some degree of freedom can be associated with it. Therefore, when the sonotrode applies the consolidation force on the welding stack, it is possible that the sonotrode tilts when using a higher force for a longer time. In that case, E1 would experience a higher pressure than the region closer to E2. Such explanation seems to be in agreement with the concentration of voids that is observed in the central region of the weld

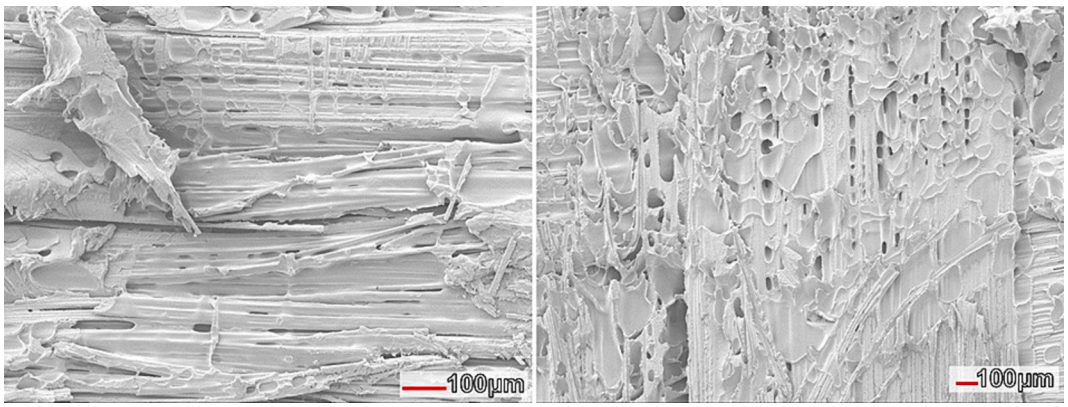

Fig. 13. SEM images of case DED-HF(A) showing a) fibres close to E1 (magnification of 100x) and b) ductile aspect of resin (magnification of 50x).

shown in Fig. 12, since the voids at E1 would collapse under the higher pressure.

5. Conclusion

Our objective with this study was to understand how changing the welding force from 500 N to 1500 N and the energy director compliance (from a continuous 0.25 mm-thick ED to a continuous 0.50 mm-thick ED and a discontinuous 0.40 mm-thick ED) affected the through-thickness heating, the size of the welded area and the optimum time of welds with C/PEEK misaligned adherends. Increasing the welding force imposes parallelism on the adherends, improving the transmission of the vibration amplitude and the uniformity of the cyclic strain on the ED. Therefore, through-thickness heating and optimum time diminished while the welded area increased. On the other hand, increasing the ED compliance improves the contact between adherends and ED, but the distribution of the cyclic strain remains rather uneven. Consequently, although through-thickness heating and size of the welded area were improved through increasing the ED compliance, the optimum time was not significantly affected. The use of a discontinuous film has an additional benefit, which is to be more efficient in focusing heat generation at the welding interface. Therefore, optimum welds obtained with a discontinuous film further diminished the through-thickness heating on the adherends in comparison to the use of a thicker ED. The best results were obtained when combining the use of a discontinuous film with the increased welding force, which resulted in the highest improvement regarding through-thickness heating on the adherends, optimum time and welded area/single-lap shear strength. Remaining voids were still observed in the welds that yielded the highest strength for all approaches. The evidences suggest that the remaining porosity is most likely caused by volatiles released during the process combined with an uneven application of the consolidation force on the welding stack as a result of the constrained downward movement of the sonotrode that occurs due to the presence of intact ED at one of the overlap's edge. These conclusions reinforce the capability of ultrasonic welding of thermoplastic composites as a robust and adaptable process to the most varied scenarios, contributing to the maturation of this technology.

Declaration of Competing Interest

The authors declare that they have no known competing financial interests or personal relationships that could have appeared to influence the work reported in this paper.

Acknowledgement

The work presented in this paper is carried out as part of a project, which has received funding from the Clean Sky 2 Joint Undertaking (JU) under the European Union's Horizon 2020 research and innovation programme under grant agreement No 776455. The results, opinions, conclusions, etc. presented in this work are those of the author(s) only and do not necessarily represent the position of the JU; the JU is not responsible for any use made of the information contained herein.

Data availability

The raw/processed data required to reproduce these findings cannot be shared at this time as the data also forms part of an ongoing study.

References

[1] Bhudolia S, Joshi S. Low-velocity impact response of carbon fibre composites with novel liquid methylmethacrylate thermoplastic matrix. Compos Struct 2018;203:696–708.
[2] Obande W, Ray D, Brádaigh CÓ. Viscoelastic and drop-weight impact properties of an acrylic-matrix composite and a conventional thermoset composite–a comparative study. Mater Lett 2019;238:38–41.
[3] Kinvi-Dossou G, Matadi Boumbimba R, Bonfoh N, Garzon-Hernandez S, Garcia-Gonzalez D, Gerard P, et al. Innovative acrylic thermoplastic composites versus conventional composites: improving the impact performances. Compos Struct 2019;217:1–13.
[4] Gardiner G. Thermoplastic composites gain leading edge on the A380; 2006. [Online].
[5] Offringa A. New thermoplastic composite design concepts and their automated manufacture; 2012. [Online].
[6] Potente H. Ultrasonic welding - principles & theory. Mater Des 1984;5:228–34.
[7] Benatar A, Gutowski T. Ultrasonic Welding of PEEK Graphite APC-2 Composites. Polym Eng Sci 1989;29.
[8] A. Yousefpour, M. Hojjati and J. Immarigeon, "Fusion Bonding/Welding of Thermplastic Composites," *J Thermoplast Compos Mater,* vol. 17, pp. 303-340.
[9] Zhang Z, Wang X, Luo Y, Zhang Z, Wang L. Study on heating process of ultrasonic welding of thermoplastics. J Thermoplast Compos Mater 2021;23:647–64.
[10] Levy A, Le Corre S, Villegas I. Modeling of the heating phenomena in ultrasonic welding of thermoplastic composites with flat energy directors. J Mater Process Technol 2014;214:1361–71.
[11] Villegas I, Grande B, Bersee H, Benedictus R. A comparative evaluation between flat and traditional energy directors for ultrasonic welding of CF/PPS thermoplastic composites. Compos Interfaces 2015;22:1–13.
[12] Palardy G, Villegas I. On the effect of flat energy directors thickness on heat generation during ultrasonic welding of thermoplastic composites. Compos Interfaces 2017;24:203–14.
[13] Jongbloed B, Teuwen J, Palardy G, Villegas I, Benedictus R. Continuous ultrasonic welding of thermoplastic composites: Enhancing the weld uniformity by changing the energy director. J Compos Mater 2019:1–13.
[14] Villegas I. In situ monitoring of ultrasonic welding of thermoplastic composites through power and displacement data. J Thermoplast Compos Mater 2015;28(1):66–85.
[15] Villegas I, Moser L, Yousefpour A, Mitschang P, Bersee H. Process and performance evaluation of ultrasonic, induction and resistance welding of advanced thermoplastic composites. J Thermoplast Compos Mater 2013;26(8):1007–24.
[16] Villegas I. Ultrasonic welding of thermoplastic composites. Front Mater 2019;291.
[17] Veldman S, Kortbeek P, Wölcken P, R H, K J. Villegas I. Development of a multifunctional fuselage demonstrator. In: Proceedings of Aerospace Europe Conference, Bordeaux, France, 25 February 2020 to 28 February 2020.
[18] Benatar A. 12 - Ultrasonic welding of plastics and polymeric composites. In: Power Ultrasonics. Woodhead Publishing; 2015. p. 295–312.

[19] Brito C, Teuwen J, Dransfeld C, Villegas I. The effects of misaligned adherends on static ultrasonic welding of thermoplastic composites. Compos - A: Appl Sci Manuf 2022.
[20] Goodfellow. Polyetheretherketone PEEK Material Information; 2020.
[21] Tateishi N, North T, Woodhams R. Ultrasonic welding using tie-layer materials. Part I: Analysis of process operation. Polym Eng Sci 1992;32:600–11.
[22] Jongbloed B, Vinod R, Teuwen J, Benedictus R, Villegas I. Improving the quality of continuous ultrasonically welded thermoplastic composite joints by adding a consolidator to the welding setup. Compos - A: Appl Sci Manuf 2022;155.